

STELLAR CLUSTER FIDUCIAL SEQUENCES WITH THE ADVANCED CAMERA FOR SURVEYS¹

THOMAS M. BROWN, HENRY C. FERGUSON, ED SMITH

STScI, 3700 San Martin Drive, Baltimore, MD 21218; tbrown@stsci.edu, ferguson@stsci.edu, edsmith@stsci.edu

PURAGRA GUHATHAKURTA

UCO / Lick Observatory, 271 Interdisciplinary Sciences Building, 1156 High Street, Santa Cruz, CA 95064; raja@ucolick.org

RANDY A. KIMBLE, ALLEN V. SWEIGART

Code 667, NASA GSFC, Greenbelt, MD 20771; randy.a.kimble@nasa.gov, allen.v.sweigart@nasa.gov

ALVIO RENZINI

ESO, Karl-Schwarzschild-Strasse 2, Garching bei München, Germany; arenzini@eso.org

R. MICHAEL RICH

Division of Astronomy, Dpt. of Physics & Astronomy, UCLA, Los Angeles, CA 90095; rmr@astro.ucla.edu

DON A. VANDENBERG

Dpt. of Physics and Astronomy, University of Victoria, P.O. Box 3055, Victoria, BC, V8W 3P6, Canada; davb@uvvm.uvic.ca

Low-resolution version. High-resolution version and machine-readable tables available upon request. To appear in The Astronomical Journal.

ABSTRACT

We present color-magnitude diagrams of five Galactic globular clusters and one Galactic open cluster spanning a wide range of metallicity ($-2.1 \lesssim [\text{Fe}/\text{H}] \lesssim +0.3$), as observed in the F606W (broad V) and F814W (I) bands with the Advanced Camera for Surveys (ACS) on the *Hubble Space Telescope*. These clusters are part of two large ACS programs measuring the star formation history in the Andromeda halo, tidal stream, and outer disk. In these programs, the clusters serve as empirical isochrones and as calibrators for the transformation of theoretical isochrones to the ACS bandpasses. To make these data more accessible to the community, for each cluster, we provide a ridge line tracing the stars on the main sequence, subgiant branch, and red giant branch, plus the locus of stars on the horizontal branch. In addition, we provide the transformation of the Victoria-Regina isochrones to the ACS bandpasses.

Subject headings: color-magnitude diagrams – globular clusters: general – globular clusters: individual (NGC 6341, NGC 6752, NGC 104, NGC 5927, NGC 6528) – open clusters: individual (NGC 6791)

1. INTRODUCTION

The Advanced Camera for Surveys (ACS; Ford et al. 1998) on the *Hubble Space Telescope* (*HST*) provides far greater broad-band optical sensitivity than its predecessor, the Wide Field Planetary Camera 2 (WFPC2). Two of the most widely used filters on the ACS Wide Field Camera (WFC) are the F606W (broad V) and F814W (I); the former provides three times the throughput of the analogous filter on WFPC2, while the latter provides five times the throughput of the corresponding filter on WFPC2. Although the F555W on ACS more closely approximates the Johnson V bandpass, the F606W has far more grasp, making it the filter of choice for deep imaging programs.

This enormous advance in sensitivity allows the *HST* to resolve the old main sequence in populations out to the edge of the Local Group, given a reasonable investment of exposure time (~ 100 orbits) and a sufficiently sparse field ($\mu_V \gtrsim 26$ mag arcsec⁻²). In order to measure the star formation history in the Andromeda halo, we used this capability to obtain extremely deep images of Andromeda in a field 51' from the nucleus on the southeast minor axis (Brown et al. 2003). In addition to

these deep images, our program included brief exposures of five Galactic globular clusters, using the same camera and filters: NGC 6341, NGC 6752, NGC 104, NGC 5927, and NGC 6528. These cluster observations serve two purposes: they provide empirical isochrones for old simple stellar populations spanning a wide range of metallicity, and they serve as calibrators for the transformation of theoretical isochrones to the ACS bandpasses. Subsequent to our first ACS program, we obtained additional observations of the Andromeda tidal stream (discovered by Ibata et al. 2001) and outer disk; this second program included an observation of the old open cluster NGC 6791 in order to expand the range of metallicities sampled in the empirical isochrones. Because these data would be useful references for other ACS programs, we tabulate here, for each cluster, the ridge lines tracing the main sequence (MS), subgiant branch (SGB), and red giant branch (RGB) stars, plus the horizontal branch (HB) loci. In addition, we describe our transformation of the Victoria-Regina isochrones (hereafter VRI; Bergbusch & Vandenberg 2001) to the ACS bandpasses. The VRI color-temperature relations have been revised recently (Vandenberg & Clem 2003), and the VRI grid has been extended to higher metallicities and lower ages (Vandenberg, Bergbusch, & Dowler 2005). The isochrone interpolation code and the models should be available from the Canadian Astronomy Data Centre later this year.

¹Based on observations made with the NASA/ESA Hubble Space Telescope, obtained at the Space Telescope Science Institute, which is operated by AURA, Inc., under NASA contract NAS 5-26555. These observations are associated with proposals 9453 and 10265.

TABLE 1: Parameters^a of Galactic clusters observed with ACS exposures

| Name | F606W (sec) | F814W (sec) | $(m - M)_V$ (mag) | $E(B - V)$ (mag) | [Fe/H] | age (Gyr) |
|------------------|----------------|----------------|----------------------|---------------------|--------|--------------|
| NGC 6341 (M92) | 0.5079,5,90 | 0.5079,6,100 | 14.60 | 0.023 | -2.14 | 14.5 |
| NGC 6752 | 0.5079,4,40 | 0.5079,4,45 | 13.17 | 0.055 | -1.54 | 14.5 |
| NGC 104 (47 Tuc) | 0.5079,6,70 | 0.5079,5,5,72 | 13.27 | 0.024 | -0.70 | 12.5 |
| NGC 5927 | 2,30,500 | 0.6934,15,340 | 15.85 | 0.42 | -0.37 | 12.5 |
| NGC 6528 | 4,50,450 | 1,20,350 | 16.31 | 0.55 | +0.00 | 12.5 |
| NGC 6791 | 0.5079,5,50 | 0.5079,5,50 | 13.50 | 0.14 | +0.30 | 9.0 |

^aSee §4 for discussion and references for these parameters.

2. OBSERVATIONS AND DATA REDUCTION

The Galactic clusters in our programs are listed in Table 1. The globular clusters were observed as part of *HST* program GO-9453, while NGC 6791 was observed as part of *HST* program GO-10265. Although the enormous sensitivity of ACS has enabled great strides in the deep imaging of faint targets, ironically, the camera sensitivity makes it challenging to observe relatively bright star clusters in our own Galaxy. We observed each cluster for one orbit, staggering the exposure times by an order of magnitude to increase the dynamic range. Due to the exposure overheads (CCD readout, buffer dumps, etc.), only six ACS/WFC images can be taken in a single orbit outside of the *HST* continuous viewing zone, allowing three images in each bandpass (F606W and F814W). For the three relatively distant globular clusters (NGC 6341, NGC 5927, and NGC 6528), we roughly centered the WFC on the cluster core, maximizing the number of stars in the samples. For the two relatively nearby globular clusters (NGC 104 and NGC 6752), we offset the ACS images from the cluster core, to include regions of lower background and higher signal-to-noise ratio for the photometry of the relatively faint main sequence stars. The nearby open cluster NGC 6791 is relatively sparse and subtends an area much larger than the ACS field of view, so we centered the WFC roughly in the cluster core.

We observed these clusters to create empirical isochrones and to calibrate the transformation of theoretical isochrones to the ACS bandpasses. The observing strategy was designed to efficiently achieve these purposes, but the data are not optimal for detailed studies of the clusters themselves. In particular, the exposures are brief (sometimes less than 1 sec), they are not split into two subexposures, nor are they dithered, thus foregoing the traditional method of cosmic ray rejection and precluding a better sampled point spread function (PSF). However, by comparing each set of cluster images, even with their different exposure times, we were able to create adequate cosmic ray masks. Note that, in 2003, the effective exposure times for commanded exposures of less than 1 sec were remeasured and updated in the *HST* calibration pipeline, such that a 0.5 sec exposure is really 0.5079 sec, and a 0.7 sec exposure is really 0.6934 sec (Gilliland & Hartig 2003). Because the images were not dithered, no large changes in plate scale were applied when the masked images were registered and coadded, as often done to better sample the PSF.

All of the images of a given cluster in a given bandpass were coadded using the DRIZZLE package (Fruchter & Hook 2002), with masking of cosmic rays, saturated pixels, and bad pixels. Although no gross changes to the plate scale were applied, this step does correct for the geometric distortion, small temporal changes in plate scale due to velocity aberration and telescope breathing, and a small difference in plate scale

between the two bandpasses. Because the images are filled with thousands of stars, we used the stellar positions in each exposure to accurately determine the shifts and scales needed to register the exposures. The DRIZZLE package also provides software for the masking of cosmic rays. We tuned the software parameters to aggressively mask cosmic rays without masking the cores of unsaturated bright stars; these masks were then confirmed by visual inspection. In the medium and long exposures, the mask for all saturated pixels (either due to a bright star or cosmic ray) was enlarged with a border of 7 pixels to mask the bleeding of saturated pixels into neighboring pixels; the short exposure suffers from very few cosmic-ray hits and very little bleeding of saturated pixels.

The five globular clusters were all observed using a CCD gain of 1 e⁻ per data number (DN), in order to match exactly the observing mode used in our deep imaging of the Andromeda halo. The observations were planned before the installation of ACS, when it was unclear how much uncertainty there would be in the relative gain corrections on the camera. Subsequent calibration programs have accurately measured the gain correction, and showed that a gain of 2 e⁻/DN offers significant advantages when observing bright stars, with little increase in quantization noise. With a gain of 1 e⁻/DN, the analog-to-digital converter (ADC) saturates at 65,535 DN, prior to the CCD full well of 84,700 e⁻, making it difficult to recover the flux from a saturated star. With a gain of 2 e⁻/DN, fluxes can be measured not only to the CCD full well, but beyond, via sampling the neighboring pixels where charge “bleeds” from the saturated pixel (i.e., e⁻ are conserved in the conversion to DN). Because a gain of 2 e⁻/DN can significantly extend the dynamic range of the CCD, we observed NGC 6791 with a gain of 2 e⁻/DN. As it turns out, the scarcity of giant stars in our chosen field made this choice somewhat moot.

The undersampled images do not lend themselves to accurate PSF-fitting; therefore, we obtained aperture photometry using the DAOPHOT package (Stetson 1987). We experimented with a range of aperture sizes, and ultimately chose two different apertures for the unsaturated and saturated stars. For the unsaturated stars, we chose a circular aperture of radius 2.5 pixels (0.125”) and a sky annulus of radii 7–18 pixels. With a gain of 1 e⁻/DN, saturated stars cannot be accurately photometered in a circular aperture because charge is not conserved, so instead we measured the flux in a circular annulus of radii 2.5–3.5 pixels, again with a 7–18 pixel sky annulus. We discarded from the catalog saturated stars that bled beyond a 2.5 pixel radius, or if they were adversely affected by bad pixels or were blended with bright neighbors. The photometry of the saturated stars was normalized to the same zeropoint as the unsaturated stars by comparing photometry of the unsaturated stars in the circular aperture and the annular aperture. The photometric catalog

was then corrected to true apparent magnitudes using TinyTim models of the *HST* PSF (Krist 1995) and observations of the standard star EGGR 102 (a $V = 12.8$ mag DA white dwarf) in the same filters, with agreement at the 1% level.

Charge transfer inefficiency (CTI) can be a problem for aging large-format CCDs in the space radiation environment, causing stars to appear fainter than they actually are. The ACS detector consists of two chips, 4144×2068 pixels each, separated by a small horizontal gap. Stars which fall closer to the gap undergo more parallel transfers when the detector is read, and thus suffer from more charge loss due to CTI. The CTI correction is approximately linear with the position of a star relative to the gap, and approximately linear with the age of the detector. The correction is larger for faint stars and smaller when there is a significant background. Because the globular clusters were all observed shortly after the ACS launch, the CTI correction for isolated stars would be negligible ($\ll 0.01$ mag), even at the faint end of the ridge lines we define for each cluster color-magnitude diagram (CMD), as discussed below. Because the globular cluster images are significantly crowded, the CTI is, in practice, even smaller than it would be for isolated stars. We thus applied no CTI correction to our globular cluster photometry. Unlike the globular clusters, NGC 6791 was observed 2.6 years after launch, and its ACS images are relatively sparse; because the CTI correction is small but not completely negligible (~ 0.01 mag near the faint limit at chip center), we applied a CTI correction to our NGC 6791 photometry, using the algorithm of Riess & Mack (2005).

Our photometry is in the STMAG system: $m = -2.5 \times \log_{10} f_\lambda - 21.1$ mag, where $f_\lambda = e^- \times \text{PHOTFLAM}/\text{EXPTIME}$, EXPTIME is the exposure time, and PHOTFLAM is 7.906×10^{-20} erg s $^{-1}$ cm $^{-2}$ Å $^{-1}$ / (e $^-$ s $^{-1}$) for the F606W filter and 7.072×10^{-20} erg s $^{-1}$ cm $^{-2}$ Å $^{-1}$ / (e $^-$ s $^{-1}$) for the F814W filter. The STMAG system is a convenient system because it is referenced to an unambiguous flat f_λ spectrum; an object with $f_\lambda = 3.63 \times 10^{-9}$ erg s $^{-1}$ cm $^{-2}$ Å $^{-1}$ has a magnitude of 0 in every filter. Another convenient and unambiguous system that is widely used is the ABMAG system: $m = -2.5 \times \log_{10} f_\nu - 48.6$ mag; it is referenced to a flat f_ν spectrum, such that an object with $f_\nu = 3.63 \times 10^{-20}$ erg s $^{-1}$ cm $^{-2}$ Hz $^{-1}$ has a magnitude of 0 in every filter. It is thus trivial and unambiguous to convert any of the data presented herein from STMAG to ABMAG: for F606W, ABMAG = STMAG -0.169 mag, and for F814W, ABMAG = STMAG -0.840 mag. Although our photometry could be transformed to ground magnitude systems (e.g., Johnson V) for comparison to theoretical isochrones as well as other data in the literature, such transformations always introduce significant systematic errors (see Sirianni et al. 2005). Instead of converting *HST* data to ground bandpasses so that they can be compared to models in ground bandpasses, it is preferable to produce models in one of the *HST* instrument magnitude systems, in either STMAG or ABMAG.

The CMDs of each cluster are shown in Figures 1 through 6, along with the ridge line spanning the MS, SGB, and RGB. Each ridge line was created by defining regions along the MS-SGB-RGB locus, and taking the median color and magnitude in each region. The size of the region was varied along the locus to allow clipping of outliers while including most of the stars appropriate for defining the ridge line. Larger regions were defined in parts of the CMD where the locus of stars is relatively linear, where the photometric scatter is significant (at the faint

end), and where stars are scarce (at the bright end). Smaller regions were needed where the locus curves significantly (otherwise the ridge line would smooth over these features), but fortunately this is also where the photometric errors are relatively reasonable and the CMD is relatively well-populated (between the turnoff and the base of the RGB). Near the tip of the RGB, where the CMD is very sparse, a mean was used instead of a median if less than 5 stars fell in the region. Figures 1–6 show, at representative locations, horizontal and vertical bars spanning the sizes of these regions used for defining the ridge lines. We have also highlighted the HB locus in each cluster; these stars were simply selected by eye from the obvious over-density of points in the vicinity of the HB. The observed fiducials (ridge line and HB locus) are difficult to determine accurately in NGC 6528, because the cluster suffers from high, spatially variable reddening (Heitsch & Richtler 1999), and in NGC 6791, due to the scarcity of stars. A dotted line in each figure indicates where stars can become saturated if they are well-centered on an ACS pixel. Note that when these ridge lines were presented previously (Brown 2005; Brown et al. 2003, 2004), the ridge lines were not shown above the saturation point, due to uncertainties in the correction for saturated stars with a gain of $1 e^-/\text{DN}$. Although we have taken care to correct the saturated stars, the correction is not as precise as the correction that can be done with a gain of $2 e^-/\text{DN}$, because one is effectively extrapolating from the wings of the PSF. The correction is also quite large at the tip of the RGB; for example, at $m_{F814W} = 10.5$ mag in the NGC 104 CMD, a star clipped at the limit of the ADC can exhibit $\sim 25\%$ less DN than the number of e^- actually generated on the ACS detector.

Although we have shown the globular cluster fiducials in several papers and conference proceedings, we have provided the tabular data to ACS observers upon request only. Publication of the tables was delayed until we obtained our NGC 6791 observations so that we could present a complete cluster dataset that extended to super-solar metallicity. It is worth noting that, in the interim, a separate group published ridge lines for these globular cluster data (Bedin et al. 2005). Besides our addition of NGC 6791, there are several differences between their work and that presented here, related to the photometric methods, handling of saturated stars, and reddening. More significantly, Bedin et al. (2005) used a magnitude system referenced to a spectrum of Vega that is older than the recent one of Bohlin & Gilliland (2004). They also compared the globular cluster data to a different isochrone set (Pietrinferni et al. 2004), and only did so for three of the globular clusters (NGC 6341, NGC 6752, and NGC 104), which is understandable, given the larger uncertainties associated with the clusters at higher metallicity. The work we present here will aid in the interpretation of past and future papers in our study of the star formation history in the Andromeda halo (*HST* program GO-9453), disk, and tidal stream (*HST* program GO-10265). It will also facilitate the analyses of other groups working with CMDs derived from the most popular ACS bandpasses (F606W and F814W). These tables are given in the following sections, where we also discuss how the ridge lines can be transformed to account for different levels of reddening.

3. TRANSFORMATION OF THE VICTORIA-REGINA ISOCHRONES

We briefly described our transformation of the VRI in Brown et al. (2004) but elaborate here. As distributed, the VRI provide, for a simple stellar population, the physical parameters (effective temperature, surface gravity, luminosity, and mass)

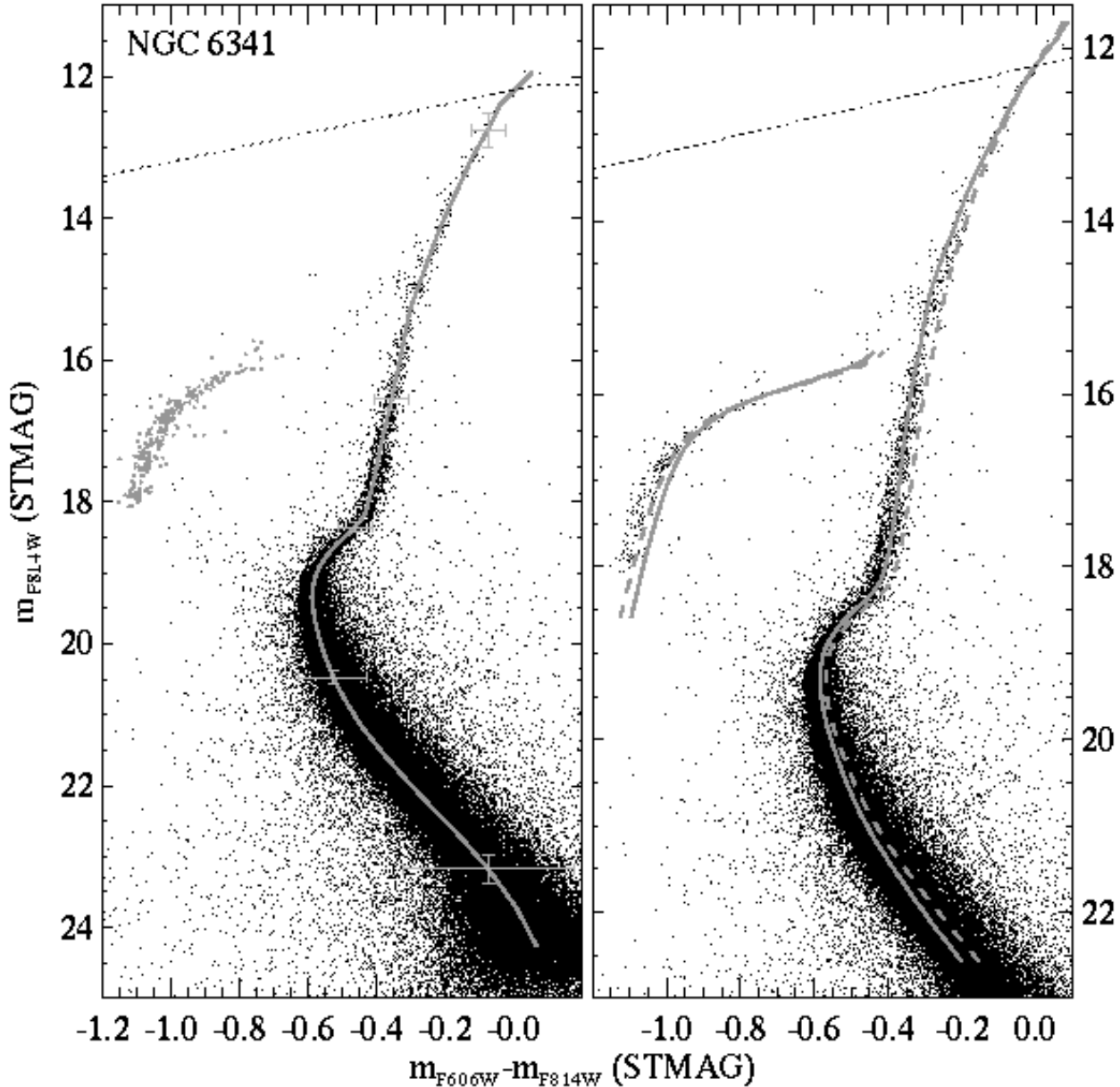


FIG. 1— *Left panel:* The CMD for NGC 6341, along with its ridge line (grey curve). The HB locus is highlighted in grey. A dashed line shows where stars can become saturated if well-centered on an ACS pixel. At representative points along the ridge line, the size of the regions used to define the ridge line are shown by horizontal and vertical lines. *Right panel:* The CMD for NGC 6341, along with an isochrone and ZAHB sequence, shown with the empirical color correction (solid curve) and without this correction (dashed curve). Note that the axes are not the same as those in the left panel, to better show the level of agreement between the models and data. The ZAHB sequence shows better agreement with the data when no empirical color correction is applied.

and the observed magnitudes in ground bandpasses (B , V , R , and I). The adopted color-temperature relations for these ground bandpasses are the ones described by Vandenberg & Clem (2003)² and, as shown by Vandenberg (2000), they yield synthetic CMDs that agree very well with the observed CMDs for a number of well-studied Galactic clusters. For this reason, Brown et al. (2003) used the synthetic spectra of Lejeune, Cuisinier, & Buser (1997) to calculate a differential transformation between the ground bandpasses and the corresponding ACS bandpasses, $V - m_{F606W}$ and $I - m_{F814W}$, for all points on the VRI, and then applied those differences to the isochrones, thus producing a set of isochrones in the ACS bandpasses. Comparison to the ACS observations of Galactic

globular clusters showed that a small empirical color correction ($\lesssim 0.05$ mag) was required to force agreement between the transformed isochrones and the observations. In a subsequent analysis of the Andromeda globular cluster SKHB-312, Brown et al. (2004) found that a direct transformation from physical parameters to ACS bandpasses (instead of the

²These transformations are nearly identical with those reported by Bell & Gustafsson (1989) for turnoff stars. At cooler temperatures, redward adjustments to the synthetic colors were applied in order that the predicted MS and RGB slopes agreed well with those observed. The color-temperature relations derived from Kurucz model atmospheres (e.g., see Castelli 1999) were used for stars hotter than ≈ 7000 K.

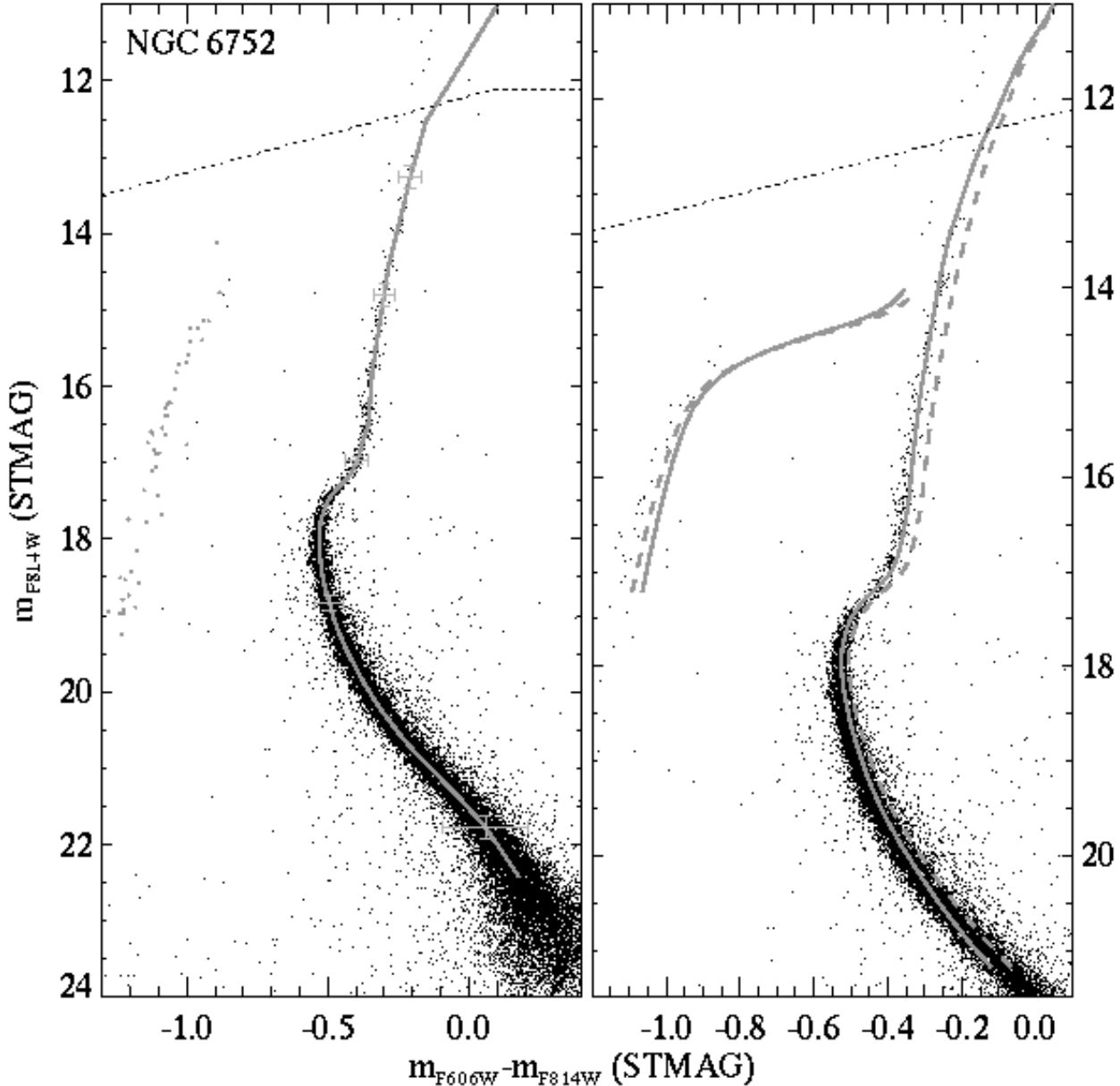


FIG. 2— The same as Figure 1, but for NGC 6752.

differential transformation above) was slightly preferable, when done in conjunction with a more extensive grid of synthetic spectra (Castelli & Kurucz 2003). The Castelli & Kurucz (2003) grid provides spectra over a wide range of metallicity, with and without alpha-enhancement, so that the chemical compositions in the spectra can be well-matched to those in the isochrones (Lejeune et al. 1997 provide only scaled-solar models). Isochrones transformed in this new direct manner, when compared to the ACS Galactic cluster data, still demonstrated the need for an empirical color correction, but it was somewhat smaller and the functional form was simpler than that required in Brown et al. (2003). In the end, the result was very similar to that obtained by Brown et al. (2003), because in both cases the isochrones were forced to agree with the same set of observational data.

To transform the isochrones to the ACS bandpasses, we first interpolate the synthetic spectra grid of Castelli & Kurucz (2003) in metallicity, effective temperature, and surface gravity

to produce a spectrum at each point on the isochrone, and then redden that spectrum using the curve of Fitzpatrick (1999). Although extinction is often handled in the literature by a “reddening vector” that is constant over the full range of a CMD, in reality the reddening produces a change in flux in each bandpass that depends upon the spectral energy distribution of the star; thus, it is more accurate to calculate the reddening at each point on the isochrone. The reddened spectrum is then converted from an energy spectrum ($\text{erg cm}^{-2} \text{s}^{-1} \text{\AA}^{-1}$) to a photon spectrum ($\text{photon cm}^{-2} \text{s}^{-1} \text{\AA}^{-1}$), multiplied by the throughput of each bandpass, and integrated over wavelength, to produce the expected count rate on the detector ($\text{e}^{-} \text{s}^{-1}$). Finally, this count rate is converted to STMAG, using the same zeropoints given in §2. Because the synthetic spectra grid of Castelli & Kurucz (2003) does not extend below 3500 K, the isochrone is truncated for any points below this temperature (near the RGB tip).

Note that the VRI do not include He diffusion, which would

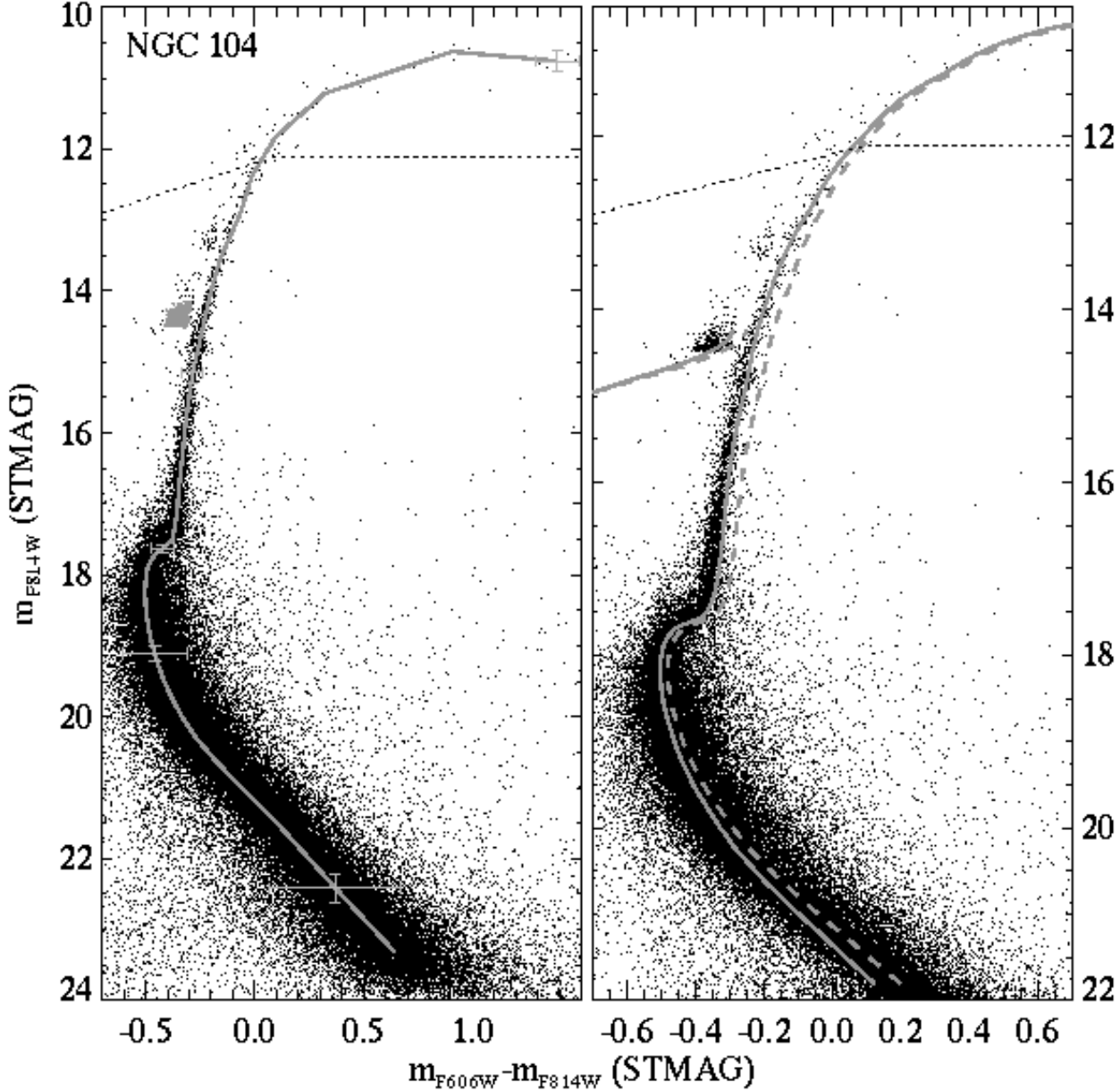


FIG. 3— The same as Figure 1, but for NGC 104.

decrease their ages at a given turnoff luminosity by $\sim 10\%$, thus avoiding discrepancies with the age of the Universe (VandenBerg et al. 2002). Although the ages of isochrones with He diffusion are likely more accurate, if diffusion is allowed to act efficiently on other elements in the surface layers, such models show significant discrepancies when compared to observed CMDs. For example, they fail to explain either the Li abundance versus effective temperature relationship obeyed by field Population II dwarfs (see Richard et al. 2002 and references therein) or the lack of any detectable difference in the derived abundances between globular cluster stars at the turnoff and on the lower giant branch (Gratton et al. 2001; James et al. 2004). Apparently, there must be some competing processes at work (e.g., turbulence at the base of the convective envelope, as invoked by Richard et al. 2002) that reduces the efficacy of diffusion in the surface layers of metal-deficient stars. However, the age effect is mainly due to the settling of He in the stellar

core, and presumably this still occurs at close to expected rates. Although the best available models to use in comparisons with stellar data are arguably those by Richard et al. (2002), which take diffusion and turbulence into account, they have (so far) been computed for only a few values of $[\text{Fe}/\text{H}]$ and only as far as the lower giant branch. In view of these considerations, it seems advisable to fit non-diffusive models to observed CMDs, and to reduce the ages so obtained by $\approx 10\%$ in order to provide the best estimates of cluster ages.

4. CLUSTER – ISOCHRONE COMPARISON

The comparison of transformed isochrones to observed clusters is not completely straightforward, because for even the most well-studied clusters, there are still significant uncertainties in their parameters: age, chemical composition, reddening, and distance. We evaluated the various values for these parameters in the literature, and settled upon those (Table 1)

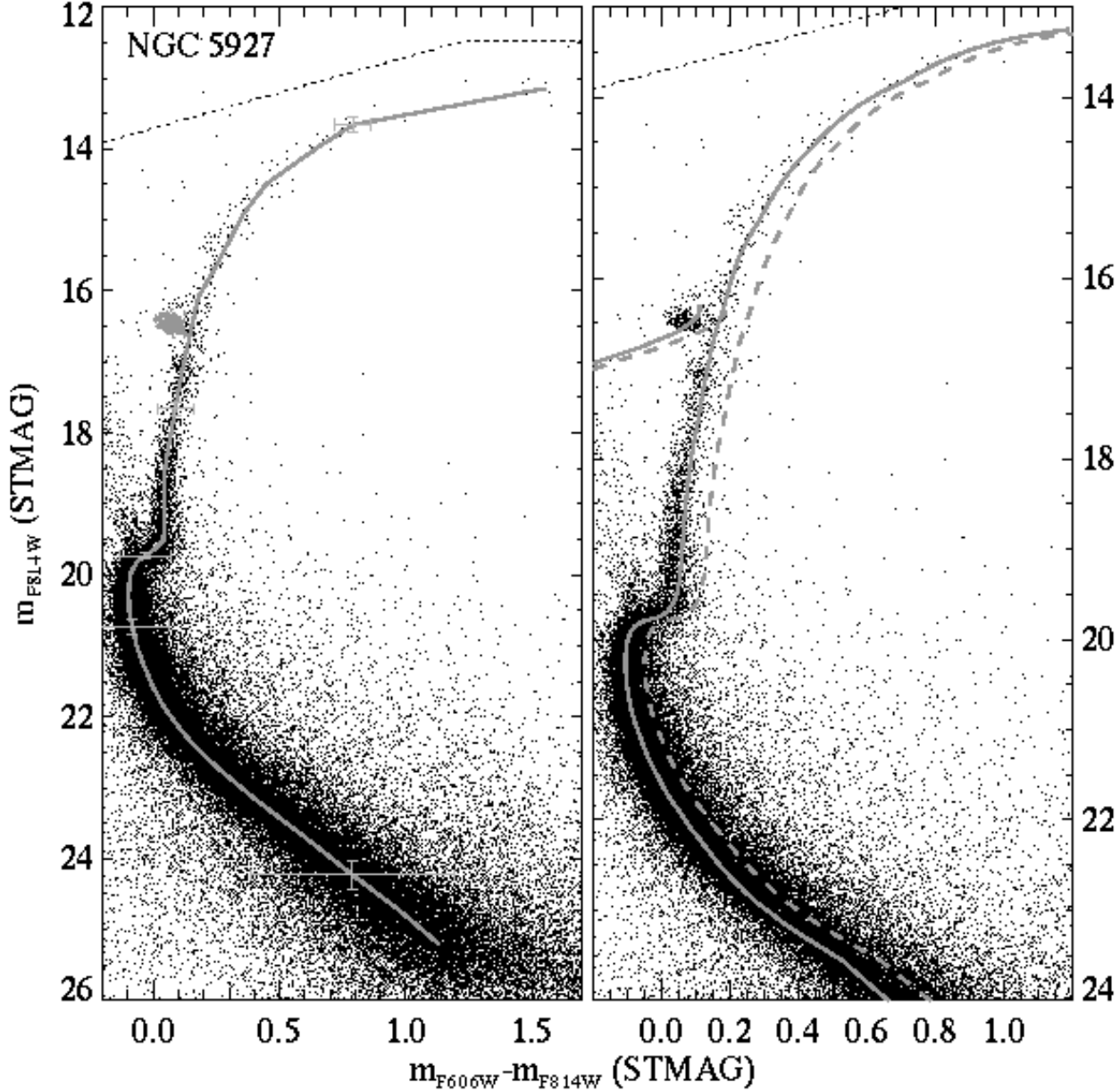


FIG. 4— The same as Figure 1, but for NGC 5927.

that minimized the empirical correction of the transformed isochrones and allowed a uniform correction for all clusters. If the same empirical correction can be applied to the transformed isochrones associated with each of these clusters, then this systematic offset can be reasonably attributed to systematic errors in the isochrones, synthetic spectra, and calibration of the bandpasses. In general, our values for the distance, $[\text{Fe}/\text{H}]$, and reddening come from the literature, while the age for each cluster is that which provides the best agreement between the ACS data and the isochrone in the vicinity of the turnoff. As distributed, the VRI interpolation code produces isochrones over a continuous range of age at discrete metallicities, but the sampling of the metallicity grid is fine enough that isochrones can be matched to clusters well within 0.1 dex. For each of the globular clusters, we compare to an isochrone with $[\alpha/\text{Fe}] = +0.3$ and a metallicity closest to that in Table 1 (see Maraston et al. 2003 for observational evidence of α -enhancement in Galactic globular

clusters over the full range of metallicity). For the open cluster NGC 6791, we interpolate the two isochrones nearest in metallicity with $[\alpha/\text{Fe}] = 0$. Note that, to first order, isochrones without alpha-enhancement look similar to isochrones with alpha-enhancement at lower metallicity; this approximation is sometimes used in the literature, although it is more accurate at lower metallicities than at metallicities near the solar value. Before comparing these isochrones to the observed CMDs, we briefly discuss the parameters we adopted for each cluster.

NGC 6341. For NGC 6341, we assumed the same distance, $[\text{Fe}/\text{H}]$, and reddening as used in Brown et al. (2003), but increased the age from 14 Gyr to 14.5 Gyr, which fits better under the new direct transformation method. Vandenberg & Clem (2003) found good agreement between the VRI and a BV CMD of M92 (Stetson & Harris 1988) when assuming $[\text{Fe}/\text{H}] = -2.14$, $E(B - V) = 0.023$ mag, $(m - M)_V = 14.60$ mag, and an age of 15 Gyr. This value of $[\text{Fe}/\text{H}]$ is very

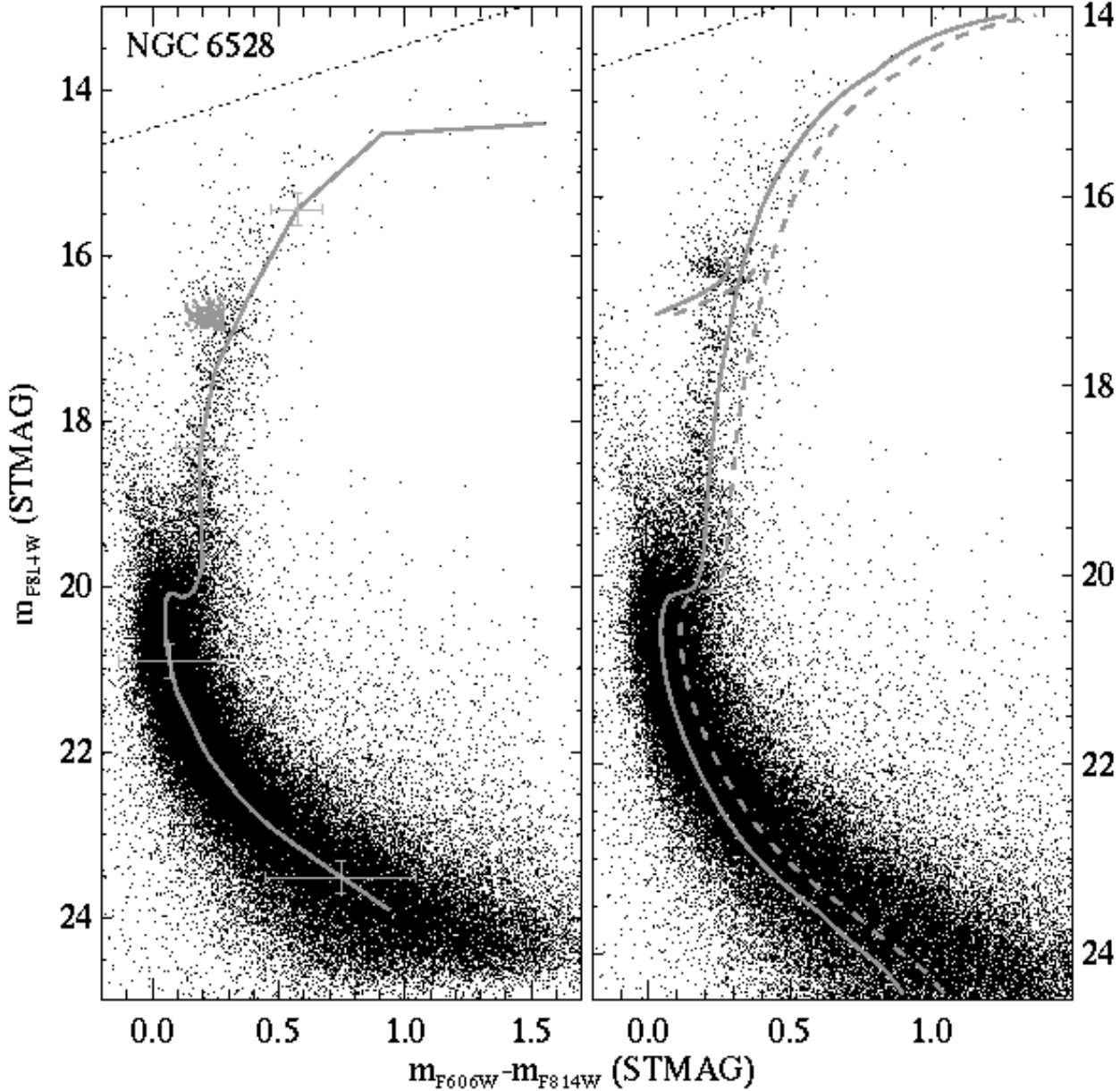


FIG. 5— The same as Figure 1, but for NGC 6528.

close to that found spectroscopically by Zinn & West (1984; -2.24 ± 0.08) and Carretta & Gratton (1997; -2.16 ± 0.02). For our comparison between the ACS data and VRI (Figure 1), we used the isochrones at $[\text{Fe}/\text{H}] = -2.14$. The extinction comes from the dust maps of Schlegel, Finkbeiner, & Davis (1998), for a sight-line through the Galaxy, which is reasonable for a distant halo cluster. The distance comes from Grundahl et al. (2000), based upon the metal-poor subgiant HD 140283; Grundahl et al. (2000) also found an age of 14.5 Gyr when performing a distance-independent fit of the VRI to Strömgren photometry of NGC 6341.

NGC 6752. For NGC 6752, we assumed the same distance, $[\text{Fe}/\text{H}]$, and reddening as used in Brown et al. (2003), but again increased the age from 14 Gyr to 14.5 Gyr, which fits better under the new direct transformation method. Vandenberg (2000) found good agreement between the VRI and the BV CMD of NGC 6752 (Penny & Dickens 1986) when

assuming $[\text{Fe}/\text{H}] = -1.54$, which is the same value found spectroscopically by Zinn & West (1984; -1.54 ± 0.09). For our comparison between the ACS data and VRI (Figure 2), we used the isochrones at $[\text{Fe}/\text{H}] = -1.54$. Renzini et al. (1996) found a true distance modulus of $(m - M)_0 = 13.05$ mag by comparison of the cluster white dwarf sequence to local white dwarfs with accurate parallaxes; they assumed an extinction of $E(B - V) = 0.04$ mag (Penny & Dickens 1986), and thus found an apparent distance modulus of $(m - M)_V = 13.17$. We have updated the extinction to $E(B - V) = 0.055$ mag, using the dust maps of Schlegel et al. (1998). Our adopted age falls in the range found in the recent literature; Renzini et al. (1996) found an age of 15.5 Gyr using non-diffusive models and 14.5 Gyr using diffusive models, while Vandenberg (2000) found an age of 12.5 Gyr, on the assumption of a somewhat larger distance modulus, using non-diffusive models.

NGC 104. For NGC 104, we assumed the same parameters

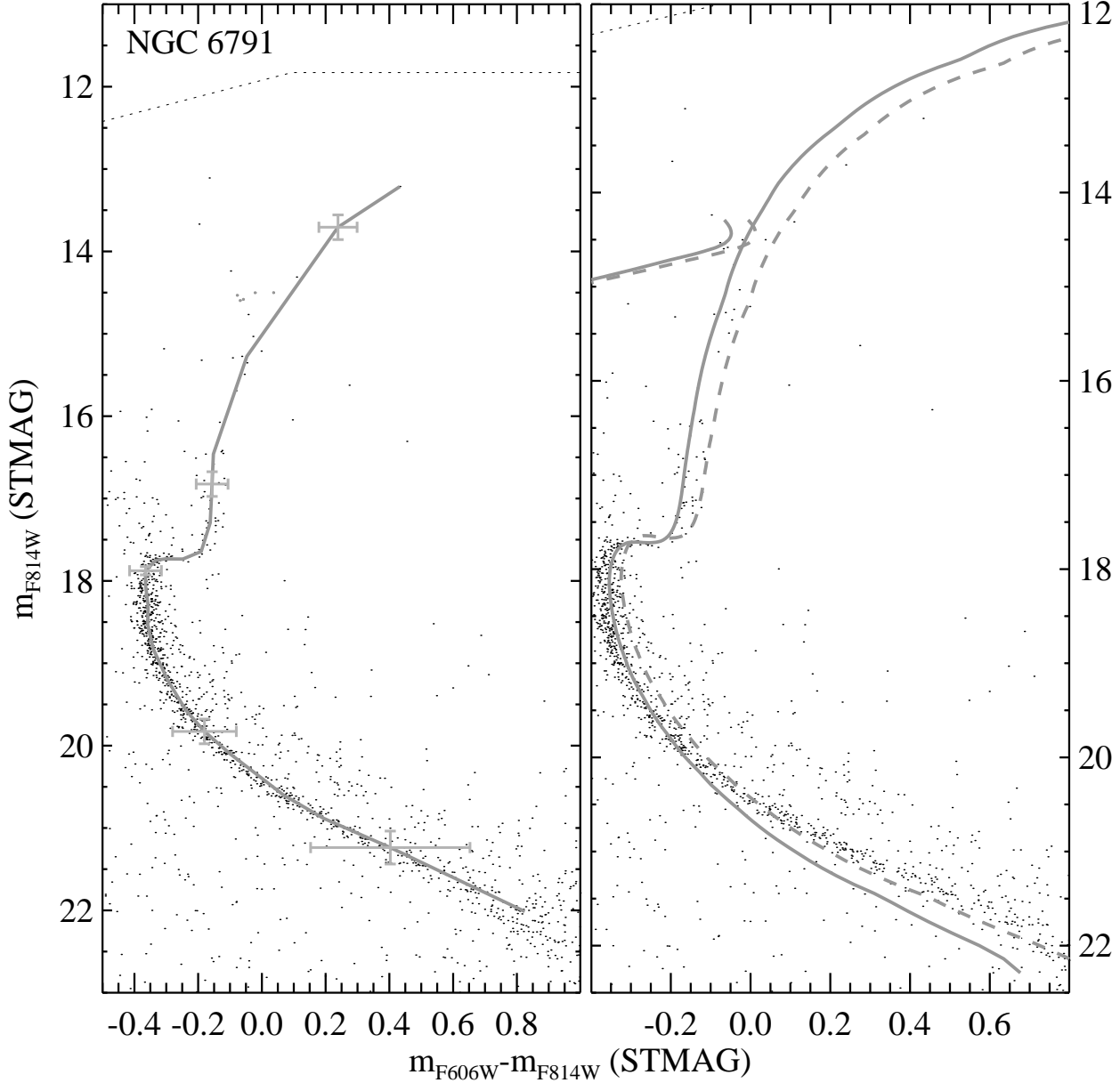


FIG. 6— The same as Figure 1, but for NGC 6791.

as those used in Brown et al. (2004). The metallicity comes from the high-resolution spectroscopy of Carretta & Gratton (1997; -0.70 ± 0.03), which agrees well with the $[\text{Fe}/\text{H}]_{\text{II}}$ fits of Kraft & Ivans (2003; -0.70 ± 0.09) and with the spectroscopic fits of Zinn & West (1984; -0.71 ± 0.08). For our comparison between the ACS data and VRI (Figure 3), we used isochrones at $[\text{Fe}/\text{H}] = -0.705$. From fits to the cluster white dwarf sequence, Zoccali et al. (2001) found an apparent distance modulus of $(m - M)_V = 13.27 \pm 0.14$ mag. Gratton et al. (2003) present several different determinations for $E(B - V)$, with an average value of 0.024 mag. Our adopted age of 12.5 Gyr is midway between that found by VandenBerg & Clem (2003; 12 Gyr), who adopted a slightly larger distance and smaller metal abundance, and Zoccali et al. (2001; 12.9 Gyr with diffusive models and 13.5 Gyr with non-diffusive models).

NGC 5927. For NGC 5927, we assumed the same parameters as those used in Brown et al. (2004). The metallicity is

that adopted by Harris (1996), and represents a combination of various spectroscopic measurements in the literature (Zinn 1985; Armandroff & Zinn 1988; François 1991). For our comparison between the ACS data and VRI (Figure 4), we used isochrones at $[\text{Fe}/\text{H}] = -0.397$. Brown et al. (2004) adopted values for distance and reddening that were slightly different from those of Harris (1996), who gives $(m - M)_V = 15.81$ mag and $E(B - V) = 0.45$ mag, but the Brown et al. (2004) values (15.85 mag and 0.42 mag, respectively) are well within the uncertainties, given the high, spatially-variable reddening (Heitsch & Richtler 1999). Our adopted age of 12.5 Gyr is also well within the wide range of ages in the literature for this cluster (see Feltzing & Gilmore 2000 for a summary of recent estimates for the age, metallicity, distance, and reddening).

NGC 6528. For NGC 6528, we assumed the same distance, reddening, and age as used in Brown et al. (2003), but we assumed a slightly higher metallicity, $[\text{Fe}/\text{H}] = 0.0$, which is still

well within the range of spectroscopic metallicities in the literature (Momany et al. 2003). For our comparison between the ACS data and VRI (Figure 5), we used isochrones at $[\text{Fe}/\text{H}] = 0$. As with the case of NGC 5927, NGC 6528 suffers from high, spatially-variable reddening (Heitsch & Richtler 1999 and references therein), resulting in considerable uncertainties in its fundamental parameters (see Feltzing & Gilmore 2000). Brown et al. (2003) found that if NGC 6528 is assumed to lie at an apparent distance modulus of $(m - M)_V = 16.15$ mag (Momany et al. 2003), the cluster, when shifted to the Andromeda distance and reddening, is too faint by 0.16 mag, implying $(m - M)_V = 16.31$ mag, which is the distance we have assumed here. We assumed the same extinction, $E(B - V) = 0.55$ mag, as found by Momany et al. (2003) in their analysis of optical and near-infrared imaging. Our adopted age of 12.5 Gyr is nearly the same as that found by Momany et al. (2003; 12.6 Gyr). Because the metallicity and reddening are very uncertain for NGC 6528, it is difficult to evaluate the empirical corrections needed to achieve agreement between the isochrone and observed CMD, but those corrections are the same as those applied to the other clusters.

NGC 6791. For NGC 6791, the Carney et al. (2005) analysis of their infrared HB photometry implies $(m - M)_V = 13.50$ mag and $E(B - V) = 0.14$ mag, and we have assumed those values here. The metallicity for NGC 6791 is quite uncertain (see Taylor 2001 for an extensive review), but Carney et al. (2005) find acceptable fits to their infrared photometry if they assume $[\text{Fe}/\text{H}] = +0.5$ (and an age of 7.5 Gyr) or $[\text{Fe}/\text{H}] = +0.3$ (and an age of 9 Gyr); we find good agreement with the latter pair of parameters. This metallicity falls midway between two metallicities in the VRI, so we interpolated between isochrones at $[\text{Fe}/\text{H}] = +0.23$ and $[\text{Fe}/\text{H}] = +0.37$; the comparison between the isochrone and ACS data is shown in Figure 6.

The comparisons between the data and isochrones are shown in Figures 1–6 (*right-hand panels*). The dashed line shows the transformed isochrone when the above steps are performed, but no empirical correction is applied. The isochrones are generally too red over much of the CMD, except for the bottom of the main sequence. Furthermore, the color difference between the turnoff and the base of the RGB is larger than observed, which may indicate, e.g., a preference either for models that treat diffusive processes and turbulence, or for models with higher oxygen abundances, as both possibilities are ways of reducing the turnoff temperatures without affecting the location of the RGB significantly. While adopting older isochrones could also alleviate this problem, the required ages are implausibly large. Because an accurate determination of the age and metallicity in a CMD generally comes from a fit of the upper MS, turnoff, SGB, and RGB, we apply a small empirical color correction, specified as a first-order polynomial:

$$(m_{F606W} - m_{F814W})_{\text{new}} = 0.92 \times (m_{F606W} - m_{F814W})_{\text{old}} - 0.06.$$

This correction gives good agreement from the upper MS to a point on the RGB slightly above the HB, but then the upper RGB increasingly deviates to the blue. Thus, we change the correction for stars at $\log g < 2$ to:

$$(m_{F606W} - m_{F814W})_{\text{new}} = 0.92 \times (m_{F606W} - m_{F814W})_{\text{old}} - 0.06 + 0.05 \times (2 - \log g).$$

This correction gives good agreement to the end of the isochrone (which, as stated above, can end before the RGB tip,

due to the 3500 K limit in the grid of synthetic spectra). In general, the transformed isochrones with the empirical correction (shown as a solid curve in the right-hand panels of Figures 1–6) agree at the $\lesssim 0.02$ mag level with the observed ridge lines from a point 1.5 mag below the MS turnoff through the upper RGB, which thus allows the isochrones to be used for fitting the age and metallicity in ACS CMDs. Over this range, the empirical correction is small ($\lesssim 0.05$ mag) but not insignificant. In the two most metal-rich clusters (NGC 6528 and NGC 6791), the agreement on the upper RGB might not be as good as that in the more metal-poor clusters, but this is difficult to evaluate, given the scarcity of stars in NGC 6791 and the high differential reddening in NGC 6528. We make no attempt to improve the agreement between the isochrones and data on the lower MS, because there is too much variation in the disagreement, from cluster to cluster, to suggest a suitable correction. Furthermore, photometry on the lower MS is not required to measure ages in CMDs (and it is beyond the reach of current instrumentation for stellar populations beyond our Galaxy and its satellites).

We also show models of the zero-age HB (ZAHB) for each cluster, again transformed using the method above. For consistency with the isochrones, the ZAHB loci were taken from Vandenberg et al. (2000); their M_V values in the center of the instability strip agree well with those derived from studies of RR Lyrae stars in Galactic globular clusters spanning a wide range in metallicity (see De Santis & Cassisi 1999; Cacciari et al. 2005). The ZAHB should trace the bottom of the HB locus, because luminosity increases during HB evolution. In general, the ZAHB models show better agreement with the data when no color correction is applied (*dashed*) than when the color correction is applied (*solid*). Although we do not use HB models in our fits of the Andromeda star formation history, it appears that a transformation of HB models to the ACS bandpasses should not employ the empirical color correction we employ in the transformation of the isochrones. Because the uncorrected ZAHB agrees well across the entire range of color, especially at the blue end, this might be indicating that a significant part of the correction required for the isochrones is driven by limitations in the synthetic spectra of stars at low effective temperature and low surface gravity, where one must account for large atomic and molecular opacities.

The transformed models for each cluster can also be used to estimate the effects of reddening on the observed fiducials, allowing them to be transformed to any given distance and reddening, for comparison to other CMDs. For example, in Brown et al. (2004), we transformed the fiducials of NGC 5927 and NGC 104 to the Andromeda distance and reddening. At each point on the fiducial, we took the closest point on the associated model, calculated the position in the CMD at both the cluster reddening and the Andromeda reddening, applied this difference to the fiducial, and then shifted by the difference in distance modulus. The absorption in each of the ACS bandpasses (A_{F606W} and A_{F814W}) is a function of both the effective temperature of the source and the foreground reddening, as parameterized by $E(B - V)$. The ratio of absorption in an ACS band to $E(B - V)$ is not constant: $R_{F606W} \equiv A_{F606W}/E(B - V)$ and $R_{F814W} \equiv A_{F814W}/E(B - V)$ are both very slowly varying functions of $E(B - V)$. For example, if one assumed that A_{F606W} at the NGC 104 turnoff was ten times larger for $E(B - V) = 1.0$ mag than it was at $E(B - V) = 0.1$ mag, this would introduce an error of 0.08 mag. Thus, the absorption in *HST* bandpasses has sometimes been published in tables giving absorption in the bandpasses at specific values of effective

temperature and $E(B - V)$ (e.g., see Bedin et al. 2005 for absorption in ACS bands and Holtzman et al. 1995 for absorption in WFPC2 bands, both specified at two distinct effective temperatures). However, using the isochrone associated with each ridge line, one can parameterize the absorption along the ridge line more generally so that it can be transformed to any reference frame. The parameterization is straightforward because R_{F606W} and R_{F814W} are nearly linear functions of $E(B - V)$, so we provide, in Tables 2–7, the ridge line for each cluster (as observed) plus the coefficients (α , β) needed to calculate R_{F606W} and R_{F814W} along the ridge line:

$$R_{F606W} = \alpha_{F606W} + \beta_{F606W} \times E(B - V)$$

$$R_{F814W} = \alpha_{F814W} + \beta_{F814W} \times E(B - V).$$

The absorption is then the product of R and $E(B - V)$. We derive these coefficients by transforming the corresponding isochrone to different values of $E(B - V)$, fitting R_{F606W} and R_{F814W} as functions of $E(B - V)$, and then matching points on the isochrone to points on the ridge line (with the isochrone at the cluster extinction). Where the ridge lines extend beyond the isochrone at the faint and bright ends of the ridge line, we simply take the closest isochrone point in the CMD. Because R_{F606W} and R_{F814W} are well-approximated by the coefficients in Table 2–7, there is little discernible difference ($\lesssim 0.01$ mag) between a transformation of the ridge line using these coefficients and the more exact method of Brown et al. (2004). In Tables 8–13, we provide the analogous data for the HB loci, again by calculating the ZAHB model at different values of $E(B - V)$, fitting the dependence of R_{F606W} and R_{F814W} on $E(B - V)$, and matching stars in the HB locus to points in the ZAHB model at the same color. We stress that the ridge lines and HB loci in Tables 2–13 present the fiducials as observed, and thus they include the reddening for each cluster (Table 1); to transform these fiducials to a different reference frame with a distinct reddening, one must first subtract the reddening intrinsic to each cluster and then add the reddening for the new reference frame, using the coefficients in Tables 2–13.

TABLE 2: NGC 6341 ridge line and reddening coefficients

| m_{F606W} (mag) | α_{F606W} (mag) | β_{F606W} | m_{F814W} (mag) | α_{F814W} (mag) | β_{F814W} |
|----------------------|---------------------------|-----------------|----------------------|---------------------------|-----------------|
| 24.346 | 2.628 | -0.077 | 24.279 | 1.709 | -0.025 |
| 23.731 | 2.628 | -0.077 | 23.724 | 1.709 | -0.025 |
| 23.103 | 2.628 | -0.077 | 23.178 | 1.709 | -0.025 |
| 22.570 | 2.628 | -0.077 | 22.726 | 1.709 | -0.025 |
| 22.090 | 2.639 | -0.078 | 22.327 | 1.712 | -0.025 |
| 21.592 | 2.654 | -0.080 | 21.909 | 1.715 | -0.025 |
| 21.194 | 2.666 | -0.082 | 21.572 | 1.718 | -0.025 |
| 20.712 | 2.679 | -0.083 | 21.159 | 1.721 | -0.025 |
| 20.248 | 2.689 | -0.084 | 20.747 | 1.723 | -0.025 |
| 19.947 | 2.695 | -0.084 | 20.475 | 1.725 | -0.025 |

Note: Table 2 is presented in its entirety in the electronic edition of the Astronomical Journal. A portion is shown here for guidance regarding its form and content.

TABLE 3: NGC 6752 ridge line and reddening coefficients

| m_{F606W} (mag) | α_{F606W} (mag) | β_{F606W} | m_{F814W} (mag) | α_{F814W} (mag) | β_{F814W} |
|----------------------|---------------------------|-----------------|----------------------|---------------------------|-----------------|
| 22.610 | 2.613 | -0.074 | 22.432 | 1.707 | -0.025 |
| 22.178 | 2.613 | -0.074 | 22.066 | 1.707 | -0.025 |
| 21.831 | 2.613 | -0.074 | 21.773 | 1.707 | -0.025 |
| 21.398 | 2.613 | -0.074 | 21.424 | 1.707 | -0.025 |
| 20.970 | 2.620 | -0.075 | 21.084 | 1.708 | -0.025 |
| 20.609 | 2.633 | -0.077 | 20.799 | 1.711 | -0.025 |
| 20.295 | 2.644 | -0.079 | 20.544 | 1.713 | -0.025 |
| 19.874 | 2.658 | -0.080 | 20.194 | 1.716 | -0.025 |
| 19.526 | 2.669 | -0.082 | 19.897 | 1.719 | -0.025 |
| 19.169 | 2.679 | -0.083 | 19.585 | 1.721 | -0.025 |

Note: Table 3 is presented in its entirety in the electronic edition of the Astronomical Journal. A portion is shown here for guidance regarding its form and content.

TABLE 4: NGC 104 ridge line and reddening coefficients

| m_{F606W} (mag) | α_{F606W} (mag) | β_{F606W} | m_{F814W} (mag) | α_{F814W} (mag) | β_{F814W} |
|----------------------|---------------------------|-----------------|----------------------|---------------------------|-----------------|
| 23.966 | 2.567 | -0.067 | 23.323 | 1.692 | -0.024 |
| 23.332 | 2.567 | -0.067 | 22.836 | 1.692 | -0.024 |
| 22.784 | 2.567 | -0.067 | 22.415 | 1.692 | -0.024 |
| 22.077 | 2.567 | -0.067 | 21.867 | 1.692 | -0.024 |
| 21.519 | 2.578 | -0.068 | 21.436 | 1.698 | -0.025 |
| 21.028 | 2.594 | -0.071 | 21.067 | 1.704 | -0.025 |
| 20.466 | 2.618 | -0.075 | 20.641 | 1.710 | -0.025 |
| 20.022 | 2.636 | -0.077 | 20.293 | 1.713 | -0.025 |
| 19.771 | 2.647 | -0.079 | 20.088 | 1.715 | -0.025 |
| 19.467 | 2.658 | -0.080 | 19.832 | 1.717 | -0.025 |

Note: Table 4 is presented in its entirety in the electronic edition of the Astronomical Journal. A portion is shown here for guidance regarding its form and content.

TABLE 5: NGC 5927 ridge line and reddening coefficients

| m_{F606W} (mag) | α_{F606W} (mag) | β_{F606W} | m_{F814W} (mag) | α_{F814W} (mag) | β_{F814W} |
|----------------------|---------------------------|-----------------|----------------------|---------------------------|-----------------|
| 26.339 | 2.560 | -0.066 | 25.207 | 1.679 | -0.024 |
| 25.678 | 2.560 | -0.066 | 24.710 | 1.679 | -0.024 |
| 25.018 | 2.560 | -0.066 | 24.229 | 1.679 | -0.024 |
| 24.284 | 2.564 | -0.067 | 23.688 | 1.685 | -0.024 |
| 23.600 | 2.579 | -0.068 | 23.188 | 1.696 | -0.024 |
| 22.972 | 2.601 | -0.072 | 22.719 | 1.706 | -0.025 |
| 22.554 | 2.618 | -0.075 | 22.396 | 1.710 | -0.025 |
| 22.204 | 2.633 | -0.077 | 22.112 | 1.713 | -0.025 |
| 21.873 | 2.647 | -0.079 | 21.837 | 1.716 | -0.025 |
| 21.546 | 2.658 | -0.080 | 21.552 | 1.718 | -0.025 |

Note: Table 5 is presented in its entirety in the electronic edition of the Astronomical Journal. A portion is shown here for guidance regarding its form and content.

TABLE 6: NGC 6528 ridge line and reddening coefficients

| m_{F606W} (mag) | α_{F606W} (mag) | β_{F606W} | m_{F814W} (mag) | α_{F814W} (mag) | β_{F814W} |
|----------------------|---------------------------|-----------------|----------------------|---------------------------|-----------------|
| 24.847 | 2.559 | -0.066 | 23.908 | 1.680 | -0.024 |
| 24.554 | 2.564 | -0.066 | 23.710 | 1.686 | -0.024 |
| 24.253 | 2.567 | -0.067 | 23.508 | 1.690 | -0.024 |
| 23.961 | 2.575 | -0.068 | 23.309 | 1.695 | -0.024 |
| 23.660 | 2.583 | -0.069 | 23.104 | 1.700 | -0.025 |
| 23.365 | 2.594 | -0.071 | 22.900 | 1.704 | -0.025 |
| 23.088 | 2.604 | -0.072 | 22.696 | 1.707 | -0.025 |
| 22.823 | 2.618 | -0.074 | 22.493 | 1.710 | -0.025 |
| 22.566 | 2.629 | -0.076 | 22.288 | 1.712 | -0.025 |
| 22.316 | 2.640 | -0.078 | 22.088 | 1.714 | -0.025 |

Note: Table 6 is presented in its entirety in the electronic edition of the Astronomical Journal. A portion is shown here for guidance regarding its form and content.

TABLE 7: NGC 6791 ridge line and reddening coefficients

| m_{F606W} (mag) | α_{F606W} (mag) | β_{F606W} | m_{F814W} (mag) | α_{F814W} (mag) | β_{F814W} |
|----------------------|---------------------------|-----------------|----------------------|---------------------------|-----------------|
| 22.838 | 2.552 | -0.067 | 22.014 | 1.670 | -0.023 |
| 22.333 | 2.559 | -0.067 | 21.687 | 1.680 | -0.024 |
| 21.640 | 2.569 | -0.067 | 21.238 | 1.690 | -0.024 |
| 21.071 | 2.581 | -0.069 | 20.880 | 1.700 | -0.025 |
| 20.667 | 2.595 | -0.071 | 20.600 | 1.706 | -0.025 |
| 20.002 | 2.621 | -0.075 | 20.102 | 1.713 | -0.025 |
| 19.647 | 2.634 | -0.077 | 19.828 | 1.716 | -0.025 |
| 19.327 | 2.645 | -0.078 | 19.567 | 1.718 | -0.025 |
| 18.905 | 2.657 | -0.080 | 19.202 | 1.721 | -0.025 |
| 18.480 | 2.666 | -0.081 | 18.822 | 1.723 | -0.025 |

Note: Table 7 is presented in its entirety in the electronic edition of the Astronomical Journal. A portion is shown here for guidance regarding its form and content.

TABLE 8: NGC 6341 HB locus and reddening coefficients

| m_{F606W} (mag) | α_{F606W} (mag) | β_{F606W} | m_{F814W} (mag) | α_{F814W} (mag) | β_{F814W} |
|----------------------|---------------------------|-----------------|----------------------|---------------------------|-----------------|
| 16.858 | 2.801 | -0.092 | 18.074 | 1.752 | -0.025 |
| 16.838 | 2.801 | -0.092 | 17.993 | 1.752 | -0.025 |
| 16.245 | 2.801 | -0.092 | 17.397 | 1.752 | -0.025 |
| 16.769 | 2.801 | -0.092 | 17.905 | 1.752 | -0.025 |
| 16.789 | 2.801 | -0.092 | 17.916 | 1.752 | -0.025 |
| 16.943 | 2.801 | -0.092 | 18.068 | 1.752 | -0.025 |
| 16.791 | 2.801 | -0.092 | 17.916 | 1.752 | -0.025 |
| 16.739 | 2.801 | -0.092 | 17.862 | 1.752 | -0.025 |
| 16.722 | 2.799 | -0.092 | 17.841 | 1.751 | -0.025 |
| 16.586 | 2.799 | -0.092 | 17.703 | 1.751 | -0.025 |

Note: Table 8 is presented in its entirety in the electronic edition of the Astronomical Journal. A portion is shown here for guidance regarding its form and content.

TABLE 9: NGC 6752 HB locus and reddening coefficients

| m_{F606W} (mag) | α_{F606W} (mag) | β_{F606W} | m_{F814W} (mag) | α_{F814W} (mag) | β_{F814W} |
|----------------------|---------------------------|-----------------|----------------------|---------------------------|-----------------|
| 17.674 | 2.802 | -0.092 | 18.954 | 1.752 | -0.025 |
| 17.740 | 2.802 | -0.092 | 18.979 | 1.752 | -0.025 |
| 17.271 | 2.802 | -0.092 | 18.507 | 1.752 | -0.025 |
| 18.010 | 2.802 | -0.092 | 19.244 | 1.752 | -0.025 |
| 17.569 | 2.802 | -0.092 | 18.797 | 1.752 | -0.025 |
| 17.696 | 2.802 | -0.092 | 18.923 | 1.752 | -0.025 |
| 17.744 | 2.802 | -0.092 | 18.967 | 1.752 | -0.025 |
| 17.315 | 2.802 | -0.092 | 18.536 | 1.752 | -0.025 |
| 16.533 | 2.802 | -0.092 | 17.741 | 1.752 | -0.025 |
| 17.530 | 2.802 | -0.092 | 18.737 | 1.752 | -0.025 |

Note: Table 9 is presented in its entirety in the electronic edition of the Astronomical Journal. A portion is shown here for guidance regarding its form and content.

TABLE 10: NGC 104 HB locus and reddening coefficients

| m_{F606W} (mag) | α_{F606W} (mag) | β_{F606W} | m_{F814W} (mag) | α_{F814W} (mag) | β_{F814W} |
|----------------------|---------------------------|-----------------|----------------------|---------------------------|-----------------|
| 14.075 | 2.678 | -0.083 | 14.484 | 1.722 | -0.025 |
| 13.874 | 2.678 | -0.083 | 14.279 | 1.722 | -0.025 |
| 14.028 | 2.678 | -0.083 | 14.432 | 1.722 | -0.025 |
| 14.056 | 2.678 | -0.083 | 14.460 | 1.722 | -0.025 |
| 13.998 | 2.678 | -0.083 | 14.400 | 1.722 | -0.025 |
| 14.028 | 2.678 | -0.083 | 14.430 | 1.722 | -0.025 |
| 14.085 | 2.678 | -0.083 | 14.485 | 1.722 | -0.025 |
| 13.940 | 2.678 | -0.083 | 14.339 | 1.722 | -0.025 |
| 14.068 | 2.678 | -0.083 | 14.466 | 1.722 | -0.025 |
| 14.074 | 2.678 | -0.083 | 14.472 | 1.722 | -0.025 |

Note: Table 10 is presented in its entirety in the electronic edition of the Astronomical Journal. A portion is shown here for guidance regarding its form and content.

TABLE 11: NGC 5927 HB locus and reddening coefficients

| m_{F606W} (mag) | α_{F606W} (mag) | β_{F606W} | m_{F814W} (mag) | α_{F814W} (mag) | β_{F814W} |
|----------------------|---------------------------|-----------------|----------------------|---------------------------|-----------------|
| 16.407 | 2.671 | -0.082 | 16.402 | 1.721 | -0.025 |
| 16.430 | 2.671 | -0.082 | 16.421 | 1.721 | -0.025 |
| 16.370 | 2.671 | -0.082 | 16.361 | 1.721 | -0.025 |
| 16.506 | 2.671 | -0.082 | 16.490 | 1.721 | -0.025 |
| 16.403 | 2.671 | -0.082 | 16.384 | 1.721 | -0.025 |
| 16.534 | 2.671 | -0.082 | 16.515 | 1.721 | -0.025 |
| 16.407 | 2.671 | -0.082 | 16.386 | 1.721 | -0.025 |
| 16.503 | 2.671 | -0.082 | 16.479 | 1.721 | -0.025 |
| 16.452 | 2.671 | -0.082 | 16.428 | 1.721 | -0.025 |
| 16.520 | 2.671 | -0.082 | 16.495 | 1.721 | -0.025 |

Note: Table 11 is presented in its entirety in the electronic edition of the Astronomical Journal. A portion is shown here for guidance regarding its form and content.

TABLE 12: NGC 6528 HB locus and reddening coefficients

| m_{F606W} (mag) | α_{F606W} (mag) | β_{F606W} | m_{F814W} (mag) | α_{F814W} (mag) | β_{F814W} |
|----------------------|---------------------------|-----------------|----------------------|---------------------------|-----------------|
| 16.784 | 2.669 | -0.081 | 16.654 | 1.720 | -0.025 |
| 16.766 | 2.669 | -0.081 | 16.636 | 1.720 | -0.025 |
| 16.728 | 2.669 | -0.081 | 16.597 | 1.720 | -0.025 |
| 16.954 | 2.669 | -0.081 | 16.818 | 1.720 | -0.025 |
| 16.981 | 2.669 | -0.081 | 16.841 | 1.720 | -0.025 |
| 16.813 | 2.669 | -0.081 | 16.670 | 1.720 | -0.025 |
| 16.835 | 2.669 | -0.081 | 16.691 | 1.720 | -0.025 |
| 16.927 | 2.669 | -0.081 | 16.778 | 1.720 | -0.025 |
| 16.876 | 2.669 | -0.081 | 16.727 | 1.720 | -0.025 |
| 16.935 | 2.669 | -0.081 | 16.784 | 1.720 | -0.025 |

Note: Table 12 is presented in its entirety in the electronic edition of the *Astronomical Journal*. A portion is shown here for guidance regarding its form and content.

TABLE 13: NGC 6791 HB locus and reddening coefficients

| m_{F606W} (mag) | α_{F606W} (mag) | β_{F606W} | m_{F814W} (mag) | α_{F814W} (mag) | β_{F814W} |
|----------------------|---------------------------|-----------------|----------------------|---------------------------|-----------------|
| 14.455 | 2.623 | -0.074 | 14.533 | 1.719 | -0.025 |
| 14.528 | 2.620 | -0.073 | 14.597 | 1.719 | -0.025 |
| 14.524 | 2.620 | -0.073 | 14.583 | 1.719 | -0.025 |
| 14.480 | 2.615 | -0.073 | 14.502 | 1.717 | -0.025 |
| 14.537 | 2.612 | -0.073 | 14.501 | 1.713 | -0.025 |

Note: Table 13 is presented in its entirety here, but for completeness a machine-readable table is available in the electronic edition of the *Astronomical Journal*, matching the format of Tables 2–12.

In Figure 7, we show all of the ridge lines and HB loci transformed to a distance of 10 pc and $E(B - V) = 0$ mag, using the information in Tables 1–13. Specifically, for each cluster, we calculated $M_{F606W} \equiv m_{F606W} - A_{F606W} - (m - M)_0$ and

$M_{F814W} \equiv m_{F814W} - A_{F814W} - (m - M)_0$, with $A = \alpha \times E(B - V) + \beta \times [E(B - V)]^2$ and $(m - M)_0 = (m - M)_V - 3.1 \times E(B - V)$. When placed in the same reference frame, the clusters fall at their expected relative locations, given their relative ages and metallicities (Table 1). Although the distances for these clusters were determined via a variety of methods, there is clear consistency in the relative distances and reddenings, given the excellent agreement at the HB. Note that the NGC 6528 and NGC 6791 photometry reaches only ~ 3 mag below the turnoff, and so their fiducials are truncated above the point where the main sequence begins to steepen (in contrast with the other clusters, which have fiducials reaching ~ 5 mag below the turnoff); this variation in depth exaggerates the impression that the fiducials are diverging at the faint limit.

5. SUMMARY

Using observations of Galactic clusters spanning a wide range in metallicity, we provide ridge lines and HB loci in the two most popular ACS/WFC bandpasses, along with coefficients for transforming these fiducials to a reference frame with an arbitrary reddening and distance. We also provide the algorithm for transforming the VRI to the ACS bandpasses, which provides good agreement ($\lesssim 0.02$ mag) with the cluster data from a point 1.5 mag below the main sequence turnoff to a point near the tip of the RGB. The empirical fiducials and the isochrone transformations should be useful in the analysis of stellar population data obtained using ACS.

Support for proposals 9453 and 10265 was provided by NASA through a grant from STScI, which is operated by AURA, Inc., under NASA contract NAS 5-26555. We are grateful to P. Stetson for providing his codes and assistance. We are also grateful to F. Castelli for making her grids of synthetic spectra available to us. We thank the members of the scheduling and operations teams at STScI (especially P. Royle, D. Taylor, and D. Soderblom) for their efforts in executing our large *HST* programs.

REFERENCES

- Armandroff, T.E., & Zinn, R. 1988, *AJ*, 96, 92
- Bedin, L.R., Cassisi, S., Castelli, F., Piotto, G., Anderson, J., Salaris, M., Momany, Y., & Pietrinferni, A. 2005, *MNRAS*, 357, 1038
- Bell, R.A., & Gustafsson, B. 1989, *MNRAS*, 236, 653
- Bergbusch, P.A., & Vandenberg, D.A. 2001, *ApJ*, 556, 322
- Brown, T.M. 2005, in *The Local Group as an Astrophysical Laboratory*, ed. M. Livio & T.M. Brown (Cambridge: Cambridge Univ. Press), 111.
- Brown, T.M., Ferguson, H.C., Smith, E., Kimble, R.A., Sweigart, A.V., Renzini, A., Rich, R.M., & Vandenberg, D.A. 2003, *ApJ*, 592, L17
- Brown, T.M., Ferguson, H.C., Smith, E., Kimble, R.A., Sweigart, A.V., Renzini, A., Rich, R.M., & Vandenberg, D.A. 2004, *ApJ*, 613, L125
- Cacciari, C., Corwin, T.M., & Carney, B.W. 2005, *AJ*, 129, 267
- Carney, B.W., Lee, J.-W., & Dodson, B. 2005, *AJ*, 129, 656
- Carretta, E., & Gratton, R.G. 1997, *A&AS*, 121, 95
- Castelli, F. 1999, *A&A*, 346, 564
- Castelli, F., & Kurucz, R.L. 2003, in *IAU Symposium 210, Modeling of Stellar Atmospheres*, eds. N. Piskunov, W.W. Weiss, & D.F. Gray, poster A20, astro-ph/0405087
- De Santis, R., & Cassisi, S. 1999, *MNRAS*, 308, 97
- Feltzing, S., & Gilmore, G. 2000, *A&A*, 355, 949
- Fitzpatrick, E.L. 1999, *PASP*, 111, 63
- François, P. 1991, *A&A*, 247, 56
- Ford, H.C., et al. 1998, *Proc. SPIE*, 3356, 234
- Fruchter, A.S., & Hook, R.N. 2002, *PASP*, 114, 144
- Gilliland, R.L., & Hartig, G. 2003, *Stability and Accuracy of HRC and WFC shutters*, *ISR ACS-2003-03*
- Gratton, R.G., et al. 2001, *A&A*, 369, 87
- Gratton, R.G., Bragaglia, A., Carretta, E., Clementini, G., Desidera, S., Grundahl, F., & Lucatello, S. 2003, *A&A*, 408, 529
- Grundahl, F., Vandenberg, D.A., Bell, R.A., Andersen, M.I., & Stetson, P.B. 2000, *AJ*, 120, 1884
- Harris, W.E. 1996, *AJ*, 112, 1487
- Heitsch, E., & Richtler, T. 1999, *A&A*, 347, 455
- Holtzman, J.A., Burrows, C.J., Casertano, S., Hester, J.J., Trauger, J.T., Watson, A.M., & Worthey, G. 1995, *PASP*, 107, 1065
- Ibata, R., Irwin, M., Lewis, G., Ferguson, A.M., & Tanvir, N. 2001, *Nature*, 412, 49
- James, G., et al. 2004, *A&A*, 414, 1071
- Kraft, R.P., & Ivans, I.I. 2003, *PASP*, 115, 143
- Krist, J. 1995, *ASP Conference Series 77, Astronomical Data Analysis Software and Systems IV*, ed. R.A. Shaw, H.E. Payne, & J.J.E. Hayes, 349
- Lejeune, T., Cuisinier, F., & Buser, R. 1997, *A&AS*, 125, 229
- Maraston, C., Greggio, L., Renzini, A., Ortolani, S., Saglia, R.P., Puzia, T.H., & Kissler-Patig, M. 2003, *A&A*, 400, 823
- Momany, Y., et al. 2003, *A&A*, 402, 607
- Penny, A.J., & Dickens, R.J. 1986, *MNRAS*, 220, 845
- Pietrinferni, A., Cassisi, S., Salaris, M., Castelli, F. 2004, *ApJ*, 612, 168
- Riess, A., & Mack, J. 2004, *Time Dependence of ACS WFC CTE Corrections for Photometry and Future Predictions*, *ISR ACS-2004-06*
- Renzini, A., et al. 1996, *ApJ*, 465, L23
- Richard, O., Michaud, G., Richer, J., Turcotte, S., Turck-Chièze, S., & Vandenberg, D.A. 2002, *ApJ*, 568, 979
- Schlegel, D.J., Finkbeiner, D.P., & Davis, M. 1998, *ApJ*, 500, 525
- Sirianni, M., et al. 2005, *PASP*, submitted
- Stetson, P.B. 1987, *PASP*, 99, 191
- Stetson, P.B., & Harris, W.E. 1988, *AJ*, 96, 909
- Taylor, B.J. 2001, *A&A*, 377, 473
- Vandenberg, D.A., 2000, *ApJS*, 129, 315
- Vandenberg, D.A., Bergbusch, P.A., & Dowler, P.D., 2005, *ApJ*, submitted

VandenBerg, D.A., & Clem, J.L. 2003, AJ, 126, 778
 VandenBerg, D.A., Richard, O., Michaud, G., & Richer, J. 2002, ApJ, 571, 487
 VandenBerg, D.A., Swenson, F.J., Rogers, F.J., Iglesias, C.A., & Alexander,
 D.R. 2000, ApJ, 532, 430

Zinn, R. 1985, ApJ, 293, 424
 Zinn, R., & West, M.J. 1984, ApJS, 55, 45
 Zoccali, M., et al. 2001, ApJ, 553, 733

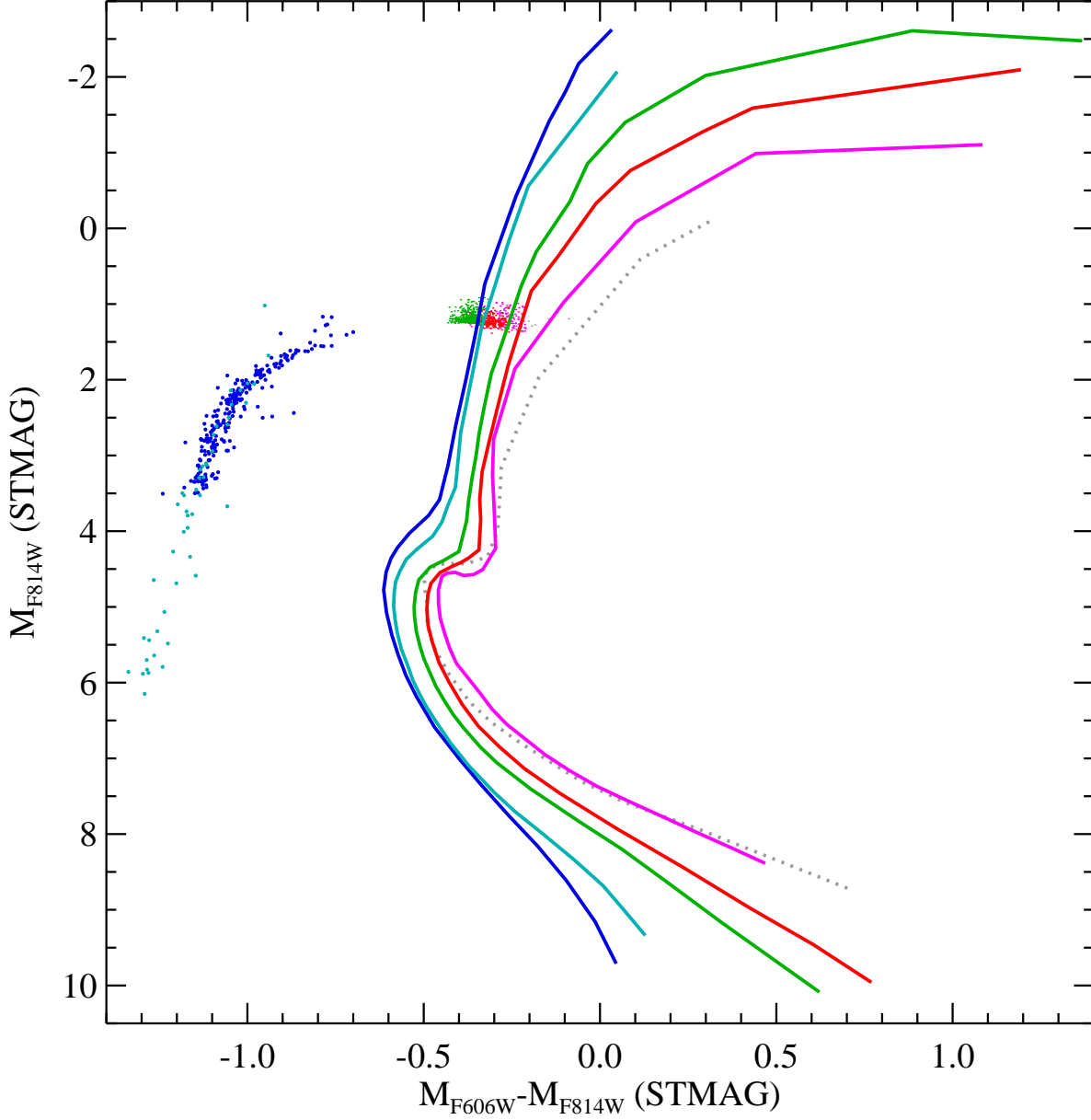


FIG. 7— The ridge lines and HB loci of Figures 1–6, shifted to a distance of 10 pc and no reddening, using the reddening coefficients of Tables 2–13 and the distance and reddening specified in Table 1. The globular cluster fiducials (*color points and solid curves*) and open cluster (*grey points and dashed curve*) fall where one would expect relative to each other, given their relative ages and metallicities (Table 1). The HB loci also show good agreement, which suggests the relative distance moduli and extinctions are consistent, even though they were derived via a variety of techniques in the literature (fitting subgiants, white dwarfs, and HB stars).